Corrosion and Enhanced Hydrogen Evolution in Electrochemical Reduction of Ammonium Carbamate on Transition Metal Surfaces

Jounghwan Choi[1,7], Shawn Chiu[2,7], Avishek Banerjee[1], Robert L. Sacci[3], Gabriel M. Veith[3], Chantal Stieber[4], Christopher Hahn[5], Anastassia N. Alexandrova[2,6,*], Carlos G. Morales-Guio[1,*]

[1] Department of Chemical and Biomolecular Engineering, University of California, Los Angeles, Los Angeles, CA 90095, USA
[2] Department of Chemistry and Biochemistry, University of California, Los Angeles, Los Angeles, CA 90095, USA
[3] Chemical Sciences Division, Oak Ridge National Laboratory, Oak Ridge, TN 37830, USA
[4] Chemistry and Biochemistry Department, California State Polytechnic University, Pomona, Pomona, CA 91768, USA
[5] Materials Science Division, Lawrence Livermore National Laboratory, Livermore, CA 94550, USA
[6] Department of Materials Science and Engineering, University of California, Los Angeles, Los Angeles, CA 90095, USA
[7] These authors contributed equally.

Abstract

Experiments and theory are combined to search for catalyst activity and stability descriptors for the direct reactive capture and conversion (RCC) of CO_2 in ammonia capture solutions using Cu, Ag, Au, Sn and Ti electrodes. Two major phenomena emerge in RCC that are not predominant in the electrochemical CO_2 reduction (CO_2R) reaction, namely, the rapid corrosion and restructuring of the catalyst in the presence of the CO_2-ammonia adducts, and the promotion of the competing hydrogen evolution reaction (HER). The prevalence of HER in RCC is correlated to the electrostatic attraction of the protonated amine to the electrode and the repulsion of the captured CO_2, using the potential of zero charge (PZC). The stability of catalysts under RCC conditions is a function of the applied potential and cannot be readily predicted using binding energy descriptors commonly used in the prediction of CO_2R activity. Three different trends are experimentally observed under RCC testing: i) Cu, and Sn corrode under open circuit potential and produce predominantly hydrogen, ii) Au and Ag show activity for the reduction of dissolved CO_2 and restructure under cathodic potentials, and iii) Ti does not corrode under open circuit conditions and only generated hydrogen as reduction product. This work shows that a direct correlation between calculated binding energies of CO_2R intermediates, atomic oxygen, hydrogen, and ammonia, and the activity and stability of transition metal for RCC cannot be found, highlighting the need for further development of activity and stability descriptors beyond those known for CO_2R.

Introduction

Capturing and upgrading CO_2 from concentrated point sources and the atmosphere using renewable electricity is a valuable approach to closing the anthropogenic carbon cycle. In existing indirect processes, CO_2 is captured, concentrated into a pure CO_2 gas stream, and then converted back to fuels and chemicals in an electrolyzer. An emerging and promising approach is to directly upgrade CO_2 from the capture media bypassing the energy-intensive CO_2 gas concentration step.[1-5] This direct route is known as reactive capture and conversion (RCC) of CO_2. RCC promises to integrate carbon capture and conversion and deliver savings in overall energy consumption and reduced capital and operating expenses primarily through the operation of the conversion step in an electrolyzer under the same conditions of temperature and pressure[6] as those utilized during the CO_2 capture step.

Traditionally, chemistries for CO_2 capture and conversion have been developed in parallel and some of the first experimental efforts in integrating these two processes have pushed the envelope beyond what is known in material science, catalysis, and engineering. Some of the first works in the electrochemical upgrading of CO_2 from amine and bicarbonate capture solutions by us and others have shown that it is the small amounts of dissolved and free CO_2 in equilibrium with the capture solutions that are being reduced electrochemically to carbon monoxide on silver electrodes.[7-10] Higher temperatures increase the partial pressure of dissolved CO_2 in equilibrium with the capture solution and lead to higher partial current densities for CO_2 reduction products at the expense of a higher thermal energy requirement.[7, 11] So far, mainly silver catalysts have been studied systematically for the electrochemical upgrading of amine and bicarbonate capture solutions, and only recently copper has been shown to be able to upgrade carbonates with Faradaic efficiencies of 0.61% under pulse electrolysis conditions.[9] In the RCC works reported so far, hydrogen evolution reaction (HER) dominates, and it is already evident that interactions of the capture agent with the catalyst increase the complexity of these systems compared to those where only CO_2 and the catalyst are considered.

Early experimental works by Hori and co-workers showed that when CO_2 is electrochemically reduced in a CO_2-saturated bicarbonate electrolyte, the product distribution can vary widely, depending primarily on the electrode metals and potentials used.[12] Metal surfaces provide the site of reaction, and the product selectivity during the electrochemical CO_2 reduction (CO_2R) depends on whether or not the reactants and other reaction intermediate species are adsorbed to the surface. Selectivity also depends on the strength of the absorption,[13] the hydrodynamics in the electrochemical cell,[14, 15] the local microenvironment, and the dynamic restructuring of the surface under CO_2R. To a large extent, the binding energy of *CO, which is a crucial reaction intermediate in CO_2R, has been accepted as a descriptor of activity and selectivity for CO_2R on transition metals.[16] The binding energy of *H (a key intermediate in HER) is also used to categorize metals' selectivity. Metals that bind *CO weakly, such as Au, Ag, and Zn, produce mostly CO. Metals that have a weak *CO binding energy and do not bind *H, such as Sn, Pb, and Cd, favor the production of formate.[16] Metals that bind *CO strongly, such as Ti, Ni, Pt, and Fe, are poor CO_2R catalysts that mostly produce hydrogen. Cu, with a moderately strong *CO binding energy, shows a high

current efficiency for CO_2R, and Cu favors the formation of >2e$^-$ reduction hydrocarbon and oxygenate products at high overpotentials, well-aligned with the Sabatier principle. In addition, *COOH and *OCHO are also regarded as key intermediates for CO_2R on transition metals, with *COOH and *OCHO binding energies serving as descriptors for CO and $HCOO^-$ production, respectively.[16, 17]

Although a great deal of research has gone into developing CO_2R activity descriptors on transition metals over the last decade, the development of descriptors for RCC has not been attempted. The complications that arise when a capture agent is present at the electrode/electrolyte interface have not been thoroughly investigated and require a detailed study of these systems. Furthermore, advancing the science and technology for the co-design of capture agents and catalysts for RCC requires the careful study of the various thermodynamic, kinetics, and transport fundamentals involved in RCC. These profiles change over the large operational space of temperature, pressure, concentration, potential, and pH likely to be encountered in an RCC device. In our opinion, a reasonable starting point is the comparison of known CO_2R electrocatalysts for the reduction of CO_2 when it is dissolved in a bicarbonate solution and when it is bound to the simplest of the amines, ammonia, as in ammonium carbamate. This will provide insights for the co-design of capture agents and catalysts in the vast chemical space of RCC.

In this work, experiments and theory are combined to elucidate similarities, differences, and challenges in advancing heterogeneous catalysis and capture media design for the direct electrochemical conversion of captured CO_2 in amine solutions. Fundamentally, this work aims to broadly delineate the scientific questions that must be considered when attempting to develop activity, selectivity, and stability descriptors for RCC.

Results and Discussion

Metal films of Cu, Ti, Au, Ag, and Sn have been tested for electrochemical CO_2 reduction in 0.2 M bicarbonate electrolytes at a constant current density of -12 mA cm^{-2}. Figure 1(a) shows the Faradaic efficiency for CO_2 reduction on these different metals. The sum of the faradaic efficiencies is higher than 96% for all these transition metals. Detailed descriptions of products and faradaic efficiencies are shown in Table S1 in the Supporting Information. Briefly, Cu produces hydrogen, formate, CO, and products resulting from the further reduction of the CO intermediate (>2e$^-$ products). Au, Ag, Ti, and Sn produce hydrogen, CO, and formate. While the major CO_2R reduction product in Au and Ag is CO, the major reduction product of CO_2R on Sn and Ti is formate. Figure S1 shows the rate of CO_2 conversion and hydrogen production for the different metals in units of mol cm^{-2} s^{-1}. In the gastight rotating cylinder electrode (RCE) cell, the maximum rates of CO_2 conversion are around 2.5 x 10^{-8} mol cm^{-2} s^{-1} for 0.2 M $KHCO_3$ electrolytes.[14] Cu, Au, and Ag approach this maximum rate of CO_2 conversion and indicate that at the applied current, these electrodes are already limited by CO_2 mass transport. HER on Au and Ag is more prominent than on Cu despite the applied potential being more negative for the Cu electrode. The high Faradaic efficiency for hydrogen evolution on Au and Ag is related to the improved transport of bicarbonate in the RCE cell, which relays protons to the surface of the electrode more effectively and more homogeneously than in any other electrochemical cell.[18, 19]

The reduction of CO_2 on Ti is not entirely limited by external mass transport at the applied potential while the rate of CO_2 reduction on Sn is higher than that expected from the maximum transport of dissolved CO_2 to the surface of the electrode. This is not an isolated observation[16] and suggests that Sn has additional pathways for the formation of formate that perhaps involve the adsorption of bicarbonates and carbonates on the surface and/or the shifting of the buffer equilibrium kinetics at the electrode/electrolyte interface to favor the release of additional dissolved CO_2 for formate production.

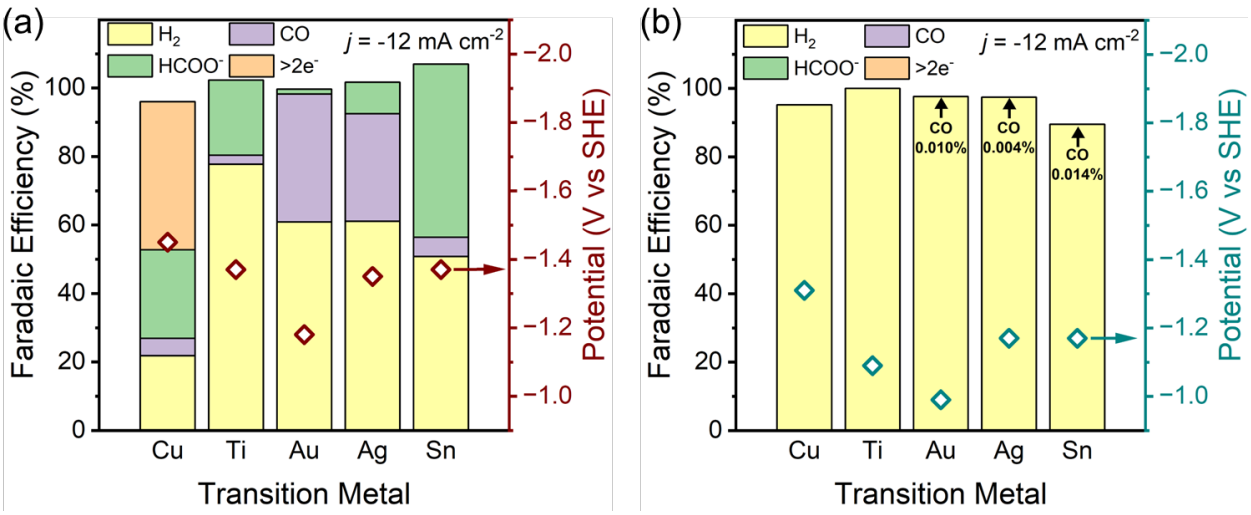

Figure 1. (a) Faradaic efficiency for electrochemical CO_2 reduction in 0.2 M $KHCO_3$ under a CO_2 flow of 20 sccm. The right y-axis shows surface potential vs SHE. (b) Faradaic efficiency for electrochemical reduction of 0.2 M ammonium carbamate under Ar flow at 20 sccm. The amine loading is 0.5 mol of CO_2 per mol of amine and is given by the stoichiometry of the ammonium carbamate used as the reactant. The right y-axis shows surface potential vs SHE. Experimental conditions: In both sets of experiments, the rotation rate of the cylinder electrode in the RCE cell is 800 rpm, the constant current passed is -12 mA cm^{-2}, and the electrochemical cell temperature is 20 °C. The partial pressure of CO_2 in the headspace of the ammonium carbamate solutions under the constant flow of Ar is in the range of 1,500 ppm (Figure S4).

The same metals tested for CO_2R were also tested for the electrochemical reduction of 0.2 M ammonium carbamate under constant Argon flow. The product observed is predominantly hydrogen (Figure 1(b) and S2), and the potentials needed to reach the same current density of -12 mA cm^{-2} under RCC conditions are less negative compared to the CO_2R study in Figure 1(b). The comparison of the applied potentials needed to reach the same currents under CO_2R and RCC conditions on these five metals is shown in Figure S2. The lower potentials recorded at the same current density under RCC conditions arise from the more facile HER that is enhanced by the presence of protonated amines in the capture solution despite the bulk pH being more alkaline under RCC conditions.[10] A trace amount of CO is observed for the Au, Ag, and Sn electrodes under RCC conditions (ca. 1,000 times less than those in the CO_2R experiments). As shown in Figure S3, the changes in Faradaic efficiency under different applied potentials are negligible, and HER is shown to be the predominant reaction in all cases. The partial pressure of CO_2 in the

headspace of the cell is roughly constant, and the current density of CO is saturated as the applied potential becomes more negative, suggesting that our RCC system is limited by the mass transport of dissolved CO_2. Furthermore, the amount of CO produced is proportional to the partial pressure of CO_2 (ca. 1,500 ppm, Figure S4), indicating that the dissolved CO_2, rather than the ammonium carbamate, is being reduced.[7] The observation of dissolved CO_2 as the source of carbon in RCC suggests that the binding constant of CO_2 to the capture agent is a system design parameter, in which the shifting of equilibrium toward dissolved CO_2 while still enabling CO_2 capture in the capture unit are desired. Importantly, CO is not observed with the Cu and Ti catalysts, indicating that although the reduction of dissolved CO_2 is thermodynamically favorable under RCC conditions, it is kinetically inaccessible in the presence of the amine on these two metals. The complete absence of CO is intriguing and perhaps explains the absence of reports using Cu and Ti as electrocatalysts for RCC in the existing literature where amines are used as the capture agents.

During the RCC experiments, we observed the dissolution of the Cu catalyst, indicated by a change in the color of the electrolyte to blue under open circuit potentials (Figure S5). UV-Vis spectroscopy reveals that the dissolved form of copper is a coordination complex between the ammonia and Cu(II) dissolved in solution, raising concerns about the long-term stability of Cu in RCC applications where amines could be used as capture agents. Although we did not observe any changes of colors in other metals, there is still a possibility that these metals dissolve in the RCC solution but give an optical response outside of the visible range of the light spectrum. The dissolution of Cu under open circuit potentials is an important realization and indicates that in addition to searching for activity and selectivity descriptors, the capture agent is non-innocent, and stability descriptors must also be developed for RCC applications.

To begin rationalizing the differences in performance and stability of RCC and CO_2R systems, we have calculated the binding energies for reaction intermediates and amine species on different metal surfaces as a function of the electrode potential using grand canonical density functional theory. The computational details are presented in the Methods section. The DFT-optimized geometries and the most favorable adsorption sites for the adsorbates are provided in Figures S6 through S10, and the approximate grand canonical free energy surfaces are shown in Figures S11 through S15. Figure 2(a) shows the potential-dependent binding energies of *CO (ΔE_{CO}) versus *H (ΔE_H) on Ag, Au, Cu, Sn, and Ti surfaces. A scaling relation between ΔE_{CO} and ΔE_H emerges for all the metals that we have tested, indicating that surfaces that bind carbon monoxide strongly will also bind hydrogen strongly. It is noted that the calculated binding energies do not take into account the adsorbate-adsorbate interactions and these coverage effects will be particularly important for metals that have strong ΔE_{CO} and ΔE_H. Trends in product selectivity during CO_2R have been attributed extensively in the literature to the favorable energetics for CO_2 activation and conversion to CO.

Firstly, our computational results reiterate what is known in the literature for the CO and H adsorption on the various metals (Figure 2(a)). Ag and Au bind CO weakly, and desorb it before reducing further, hence reducing CO_2 to CO predominately. Moreover, since these metals have similar ΔE_{CO} and ΔE_H, hydrogen production is favored as HER is much more kinetically accessible

than CO_2R. Next to the CO group is the >2e$^-$ products group, and the only known pure metal in this group is Cu. Cu has a unique, optimal ΔE_{CO} that is neither too strong nor too weak relative to other metals. This widely acknowledged characteristic enables Cu to catalyze further reduction of the *CO intermediate. Therefore, although Cu has similar ΔE_{CO} and ΔE_H, Cu can still efficiently and selectively catalyze CO_2R and produce only a small amount of hydrogen.

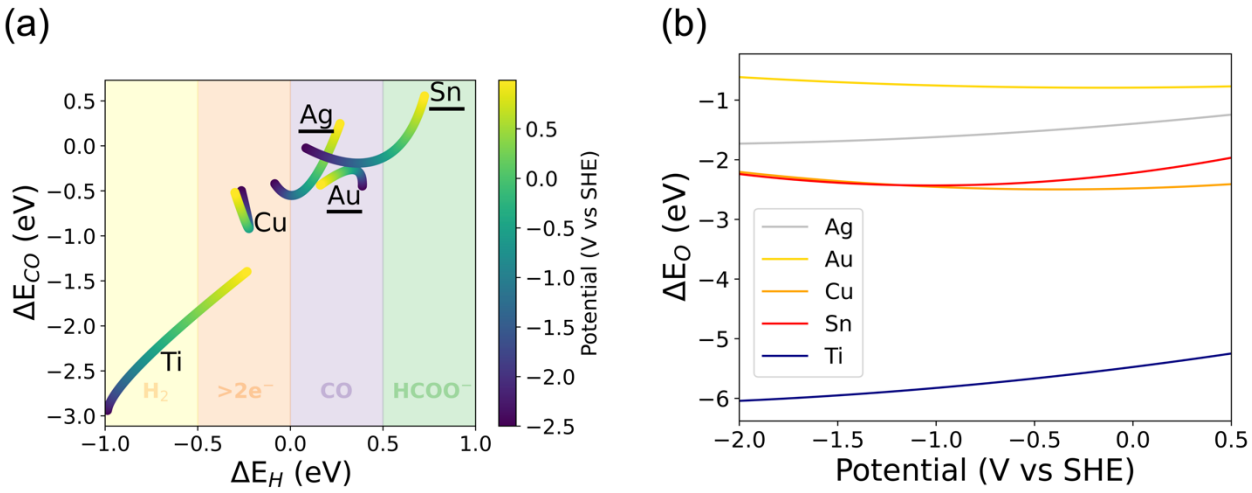

Figure 2. (a) The binding energies of *CO (ΔE_{CO}) versus *H (ΔE_H) as a function of potential for Ag, Au, Cu, Sn, and Ti. The CO and H_2 gas phase references are used. The metals that produce CO in the RCC experiments are underlined. (b) The binding energy of *O (ΔE_O) as a function of potential for Ag, Au, Cu, Sn, and Ti. The O_2 gas phase reference is used.

The rightmost group in Figure 2(a) consists of metals that mainly produce formate in CO_2R, which includes Sn. Compared to Ag and Au in the CO group, Sn has a similar ΔE_H but weaker ΔE_{CO}; therefore, Sn produces roughly the same amount of hydrogen as Ag and Au. However, the *CO intermediate is thermodynamically difficult to form on Sn in CO_2R, rendering the carbon-bound CO_2R pathway unlikely as the initial step is hindered. Previous work has proposed that CO_2 binds to the Sn electrode surface via the oxygen atoms instead of the carbon, which leads to a pathway for formate production that does not involve the *CO intermediate.[18] To probe the formate pathway, the adsorption energies of the oxygen-bound *OCHO intermediate (ΔE_{OCHO}), which has been proposed to be a key descriptor for formate production,[17] are calculated using regular DFT, and the results are shown in Figure S16. Sn has a moderate ΔE_{OCHO} compared to other metals, indicating that it can optimally stabilize the adsorption of CO_2 via the oxygen bonds, favoring the formation of oxygen-bound intermediates that lead to the production of formate predominately. Cu has a similar ΔE_{OCHO} as Sn, which can explain the noticeable formate production seen in Cu during CO_2R.

The leftmost group in Figure 2(a) is characterized by strong ΔE_{CO} and ΔE_H, and metals in this group produce predominately hydrogen.[16] Ti is placed in this group based on its faradic efficiencies and binding energies. The potential-dependent binding energy of *O (ΔE_O) is computed as shown in Figure 2(b). ΔE_O correlates with the oxophilicity of the metals,[21] with Ti being the most oxyphilic and Au the least, which is associated with the increased selectivity of Ti

towards formate.[18] Moreover, the optimal oxygen binding strength of Sn and Cu also explains the stabilization of oxygen-bound intermediates, which leads to formate production. Due to its strong ΔE_O, Ti must exist as an oxidized form rather than a metallic state, and this claim is consistent with the presence of oxide suggested in the Ti-H_2O Pourbaix diagram.[22] In previous DFT calculations, defected anatase showed ΔE_{CO} in the range from 0.1 to -0.1 eV in the potential between 0 and -0.6 V vs SHE. [23] However, the precise degree of oxide oxidation of Ti in RCC conditions is unknown, and will be a subject of future studies that are beyond the scope of this paper. Hence, computational study of Ti is omitted from further discussion here.

In the RCC experiments, all metals produced hydrogen almost exclusively (Figure 1(b)) at a lower overpotential due to the presence of the charged, protonated amine in the electrolyte that facilitates HER. A trace amount of CO is found in Au, Ag, and Sn, and these metals are underlined in Figure 2(a). They all have positive ΔE_H at the applied potential, suggesting that the unfavorable adsorption of hydrogen can provide a gateway to reduce CO_2 despite the fierce competition of HER in RCC. To investigate the dynamics of adsorption in RCC, the binding energies of the involved amine species are calculated, as shown in Figure 3. The binding energies of the protonated ammonium cation (ΔE_{NH4+}, solid lines), CO_2-captured carbamate anion ($\Delta E_{H2NCO2-}$, dotted lines), and detached CO_2 (ΔE_{CO2}, dashed lines) are plotted as a function of potential for Ag, Au, Cu, and Sn. The potential of zero charge (PZC) for each metal is plotted with vertical dash-dotted lines. PZC is an important parameter to quantify the charge transfer and electrostatics in the screening of CO_2R electrocatalysts,[24] especially when the charged species are present in RCC. The PZC for each metal corresponds to the maximum on the free energy surfaces of the pristine slab as a function of charging, shown in Figures S11 through S15. The applied potential to reach -12 mA cm^{-2} in the RCC experiments (Figure 1(b)) is marked with a triangle on the respective ΔE_{NH4+} curve.

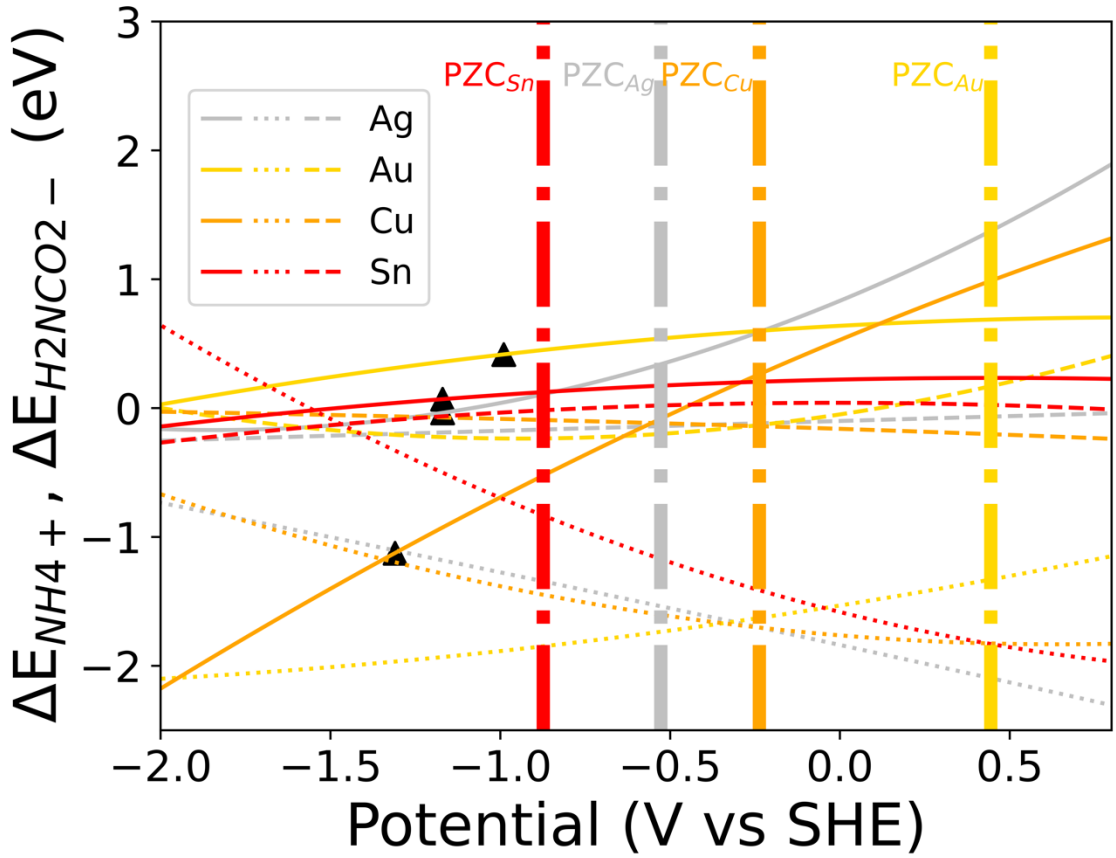

Figure 3. The binding energies of ammonium cation NH_4^+ (ΔE_{NH4+}, solid lines), carbamate anion $H_2NCO_2^-$ ($\Delta E_{H2NCO2-}$, dotted lines), and detached CO_2 (ΔE_{CO2}, dashed lines) as a function of potential for Ag, Au, Cu, and Sn. The potential of zero charge (PZC) for each metal is plotted with a vertical dash-dotted line. The applied potential to reach -12 mA cm^{-2} in the RCC experiments (Figure 1(b)) is marked with a triangle on the respective ΔE_{NH4+} curve.

As shown in Figure 3, the applied potentials to reach -12 mA cm^{-2} are more negative than the PZC of Ag, Au, Cu, and Sn, so the solvated NH_4^+ would accumulate on the electrode surfaces during RCC. For Ag, Au, and Sn at the applied potentials, ΔE_{NH4+} is comparable to ΔE_{CO2}, implying a similar thermodynamic preference for the adsorption of both $*NH_4^+$ and $*CO_2$. However, the HER stimulated by protonated amine is more kinetically favored than the CO_2R by dissolved $*CO_2$, leading predominantly to hydrogen production with only minimal CO formation as shown in Figure 1(b). Contrasting with these metals, Cu exhibits a significantly stronger ΔE_{NH4+} compared to ΔE_{CO2} under negative potentials, favoring the adsorption of protonated amine exclusively and resulting in the prevalence of HER and the absence of carbon-based products. Under the applied potentials, the partially solvated NH_4^+ can be adsorbed specifically to the electrode in the inner Helmholtz plane due to the favorable electrostatics, becoming an excellent proton source to promote HER while also blocking the active site of RCC. For all the tested metals in general, NH_4^+ tends to dominate due to the favorable electrostatics and kinetics of HER, leading to the observed predominant hydrogen production. Combined with the results shown in Figure 2(a), in which only the metals with positive ΔE_H can produce a trace amount of CO, we believe that the characteristic

of unfavorable hydrogen adsorption can lead to a less pronounced enhancement of HER relative to the metals with stronger hydrogen adsorption. A hypothesis for this phenomenon is that metals with weak hydrogen adsorption can enable outer sphere electron transfer between the electrode and the CO_2/CO_2-adduct, or the double layer is structured differently which improves the transport of the detached CO_2 to the electrode.

While HER predominates in the RCC experiments, Figure 3 shows a stronger preference for adsorbing $*H_2NCO_2^-$ over $*NH_4^+$ across all tested metals, as indicated by greater $\Delta E_{H2NCO2-}$ (not accounting for entropic effects and the transport through the double layer). However, this does not guarantee actual adsorption due to the electrostatic barrier that prevents the transport of the negatively charged $*H_2NCO_2^-$ to the electrode under reducing conditions, leading to negligible RCC activity.

The favorable enthalpy of adsorption of $*H_2NCO_2^-$ (Figure 3) suggests that other factors such as orbital interactions and polarization effects might compensate for the electrostatic repulsion. To investigate the chemical bonding origin of this, the charge transfer (CT) within the system is analyzed using Bader analysis as a function of electrochemical potential, as depicted in Figure S17. When comparing the CT across all tested metals, CT from the metal to the $*NH_4^+$ increases linearly with the applied negative potentials, while CT from $*H_2NCO_2^-$ to the metal decreases linearly. Generally, the slope of CT is steeper for $*H_2NCO_2^-$ than for $*NH_4^+$, implying more bonding interactions in $*H_2NCO_2^-$ and resulting in stronger $\Delta E_{H2NCO2-}$ compared to ΔE_{NH4+}. This difference is attributed to ammonium's smaller polarizability and the greater carbamate's orbital overlap with the surface. Hence, despite the electrostatic repulsion upon approach, $*H_2NCO_2^-$ can be stabilized through chemical bonding once adsorbed. It is not possible to fully differentiate the metals in their ability to bind carbamate in this study, without also considering transport and the structure of the electric double layer. Further research that likely requires a rigorous investigation of the electrochemical double layer with explicit solvation is needed, as enabling the reduction of captured CO_2 while limiting HER activity from the capture agent is a major roadblock in RCC that needs to be overcome (Supplementary Note 1).

Concerning HER, the transport of ammonium to the cathode must be favorable due to electrostatics. Upon adsorption, for Sn, the CT with $*NH_4^+$ is negligible, suggesting physisorption governed by electrostatics, as indicated by the constant ΔE_{NH4+} values regardless of potentials shown in Figure 3. Ag and Au exhibit lower CT levels than Cu but greater than Sn, and have flat ΔE_{NH4+} curves, also implying primarily electrostatic interactions. In contrast, Cu displays substantial CT with $*NH_4^+$, leading to a strong ΔE_{NH4+} and favoring HER exclusively, as seen in the experiment.

The corrosion of metals in the presence of amines is studied extensively in the CO_2 capture technology, and it is often circumvented through the addition of corrosion-inhibitors.[25] Although the addition of additives that protect the capture agent from thermal degradation is well established,[26, 27] it is unknown whether those inhibitors can be applied to RCC directly. To aid this development, we investigated the corrosion rates in the presence of ammonium carbamate at different potentials using an electrochemical Quartz Crystal Microbalance (eQCM) with an active

area of 1 cm^2. Studying the potential-dependent corrosion rates of the various transition metals will be important since the applied potentials play an important role in the formation of the electrochemical double layer, the stabilization of reaction intermediates, the restructuring of the surface, and presumably the barriers for CO_2-adduct activation.

The galvanostatic corrosion rates for Cu, Ti, Au, Ag, and Sn at a current of -1 μA (near the open circuit potential, OCP) and -1 mA (representative of potentials under catalytic conditions) are shown in Figure 4. At OCP, Cu and Sn have mass change rates ranging from about -0.002 to -0.005 μg cm^{-2} s^{-1}, and negligible mass change rates are observed for Ti, Au, and Ag. The comprehensive changes in mass and potential observed during each experiment as a function of time are depicted in Figure S17. Based on the Pourbaix diagrams, Cu, Sn, and Ti exist as Cu_2O, SnO_2, and TiO_2, respectively, in water at 25 °C and relevant pH near the OCP value measured with the potentiostat.[25] While these oxide layers can serve as passivation layers, Cu and Sn films still corrode upon the addition of ammonium carbamate in the solution. Previously, it has been shown that ammonia can induce the complexation of Cu ions, which significantly reduces the corrosion resistance of Cu films.[28, 29] Cu can be corroded in the Cu-NH_3-H_2O system as Cu(II) is the most thermodynamically stable form of the metal in the RCC solution.[30, 31] For Sn, although passivation in water is possible owing to the formation of an oxide layer, achieving complete passivation is unlikely as it requires the formation of a fully compact and adherent oxide film. It has been reported that the corrosion of Sn can occur in an aqueous ammonia solution, despite the presence of an oxide layer on its surface.[32] Preventing corrosion in Sn might be challenging under RCC conditions as the passivation layer is contingent upon the quality and integrity of the oxide layer. In contrast, corrosion of Ti is not observed although an oxide surface is also formed in solution for this metal. The negligible mass change of Ti and negative mass change rates of Cu and Sn indicate that the capture agents might react differently with the oxide layer depending on the identity of the metal. Au and Ag are in their metallic states at OCP, which makes them immune to corrosion.[22] This metallic form of Au[33] and Ag[34] are well documented for exhibiting almost no reactivity with ammonia at room temperature, which is in agreement with the eQCM results.

At reductive potentials, corrosion is not observed in any of the five metals. The mass change rates are all roughly zero at potentials between -1.0 and -1.3 V vs SHE. Cu, Ag, Au, and Sn are immune to corrosion since they are in the metallic state, while Ti is still likely to be protected by a titanium oxide passivation layer.[22] Although Ag and Au do not corrode and we do not see any mass change in the eQCM studies, we had previously reported the change in morphology of electrodeposited Ag films under RCC conditions.[7] The changes in morphology for the nanostructured Ag films were accompanied by changes in the visual appearance of the electrode that take place in a timescale of 5 to 10 minutes, even before reliable product quantification from the headspace of the cell is possible. The restructuring of electrodeposited Au films is not readily observed by the naked eye but changes in morphology can be observed when comparing scanning electron microscope (SEM) images of the electrodeposited Au films before and after testing (Figure S18). Surface restructuring is not evident for the sputtered films utilized in the RCC experiments shown in this work, but are readily observed for porous electrodeposited catalysts. We anticipate that surface

corrosion and surface restructuring are omnipresent in RCC systems and need to be fully considered in the development of activity descriptors. The exposure of a catalyst to an RCC solution under OCP conditions could be enough to change the catalyst from its as-synthesized form and requires careful characterization of the catalyst prior, during and after electrocatalytic testing. Restructuring of catalysts under CO_2R has been well-documented and could be potentially more significant during RCC.

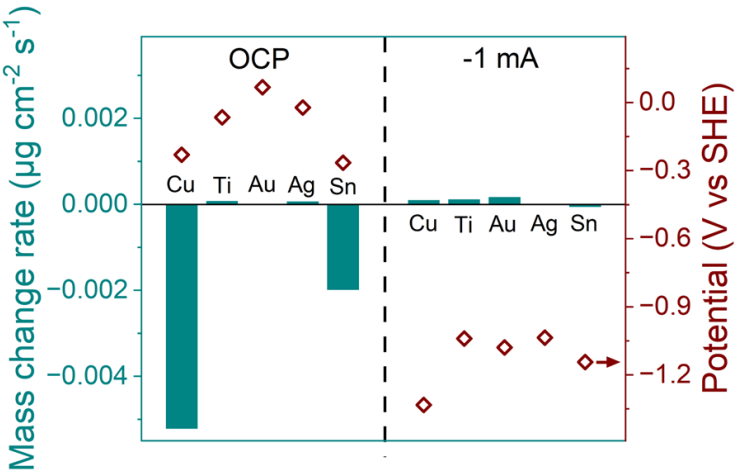

Figure 4. The mass change rates and measured potentials of sputtered Cu, Ti, Ag, Au, and Sn films after the exposure to ammonium carbamate near the open circuit potential and under a current density of -1 mA cm^{-2}.

Conclusions

In summary, we have tested and compared CO_2R in a 0.2 M bicarbonate electrolyte against RCC in a 0.2M ammonium carbamate solution on Cu, Ti, Ag, Au, and Sn electrodes. Approximately 100% of Faradic efficiencies are observed in all experiments using an RCE cell with well-defined transport characteristics and precise control of the transport of properties. Using ΔE_{CO} and ΔE_H as descriptors, the metals can be categorized based on their major carbon-based products in CO_2R. Although the major product in RCC is hydrogen, a trace amount of CO was observed in Ag, Au, and Sn electrodes that are assigned to the reduction of free and dissolved CO_2 in equilibrium with the ammonium carbamate. The electrodes that generated CO in the RCC experiments have positive ΔE_H, while the electrodes that only produced hydrogen have negative ΔE_H. ΔE_H was identified as an important descriptor in RCC, as it can describe the extent of proton adsorption on the electrode and the competition between CO_2R and HER. The requirement for more negative potentials to reduce CO_2 than the PZC of tested metals leads to an accumulation of positively charged protonated amines on the electrodes. This promotes the kinetically favored HER. Our findings suggest that when protonated amine adsorption is thermodynamically preferred over dissolved CO_2, as observed with Cu, the resulting product is exclusively hydrogen. Therefore, the dominance of HER in RCC is attributed to the presence of protonated amine.

Design strategies such as hindering proton adsorption by surface modifications and tuning the PZC of the metals by alloying should be employed to achieve optimal performance in RCC.

Furthermore, the observation of corrosion in Cu and Sn metal catalysts near the open circuit potentials reveals the complex interactions between the adsorbates and catalysts; thus, in addition to searching for activity and selectivity descriptors, stability descriptors must also be developed for RCC applications. This work shows that although some knowledge can be transferred from CO_2R to RCC, major differences emerge in the description of interactions between capture agents and catalysts which had not been elucidated before.

Alternatively, new families of capture agents with fundamentally different chemistries should be evaluated for RCC. The generation of the protonated amine is intrinsic to the chemistry of CO_2 capture with amines (e.g., 2 amines are required to capture 1 molecule of CO_2), and as shown in this work, the generated protonated amine is an excellent proton donor for HER which is the competing surface reaction. Phenoxides and alkoxides,[35] for example, could be potential capture agents that merit further exploration as these do not generated an equivalent protonated species upon capture of CO_2.

Our exploration represents just a glimpse into the vast chemical space of RCC systems. To glean fundamental insights into the co-design of RCC sorbents and catalysts, a precise depiction of electrochemical interfaces is imperative. This entails capturing surface interactions, local electrolyte concentrations, double-layer compactness, charge transfer mechanisms, bonding dynamics, non-covalent interactions, solvent cage structure, and beyond. Many of these factors are intrinsically coupled, necessitating a collaborative effort between experimentalists and theorists to navigate the complexity effectively. Experimentally, isolating and varying each controlled variable independently offers a methodical approach to scrutinizing the system's response. By categorizing results into fewer independent groups, we can reduce the dimensionality and streamline the analysis. On the theoretical front, leveraging machine learning models to extract appropriate descriptors from experimental data can expedite screening and inverse design processes for RCC. Moreover, advancements in machine learning hold promise for efficiently sampling complex surface reconstructions and diverse adsorbate coverages.

Methods

Slab model setup and DFT methods. The (111) surface of Ag, Au, Cu, Sn, Ti, and Zn electrodes were modeled by a supercell of (111) terminations of the corresponding metals with a cell dimension of roughly 15 Å × 15 Å. Terminations are obtained by cutting along the (111) plane of the bulk crystal structures obtained from the Materials Project.[36] The bottom half layers of each slab were constrained as the rigid interior, while the upper half layers were allowed to relax as the catalytic interface. A vacuum of 15 Å was added under the periodic boundary condition.

DFT calculations were performed in the VASP program (version 5.4.4) using the RPBE GGA functional[37] with DFT-D3[38] method of dispersion correction and PBE_PAW[39] pseudopotentials. The cutoff energy for the plane-wave basis set was set to 400 eV, and a Gaussian smearing with a width of 0.1 eV was used. The convergence criteria for electronic minimization and geometry optimization were set to 10^{-6} eV and 0.02 eV/Å, respectively. Due to the large supercell used in the simulation, only Γ-point sampling in the reciprocal space of the Brillouin zone was used.

Grand canonical DFT (GCDFT) calculations. To calculate the adsorption energy of the descriptors under an applied potential, the catalytic interface of the electrode was treated as a grand canonical ensemble of electrons with different amounts of charge present in the system to sample the free energy surface. The surface charging technique[40] is used to calculate the potential dependent, grand canonical free energy of the surface, ΔG, which is given by

$$\Delta G(U^{VAC}) = \Delta E^{elec}(U^{VAC}) - q(U^{VAC})FU^{VAC}$$

where $\Delta E^{elec}(U^{VAC})$ is the electronic energy at potential U^{VAC}, the vacuum scale potential of the electrode, q is the number of supplied charge to the neutral system, and F is the Faraday constant. By treating the catalytic interface as an ideal capacitor, ΔG can be approximated by

$$\Delta G(U^{VAC}) \approx \Delta E^{elec}(U_0^{VAC}) - \frac{1}{2}C(U^{VAC} - U_0^{VAC})^2$$

where U_0^{VAC} is the vacuum scale zero charge potential and C is the effective capacitance. U^{VAC} is converted to the potential with respect to the standard hydrogen electrode, U^{SHE}, as

$$U^{SHE} = U^{VAC} - 4.44$$

VASPsol[41] is used to represent the polarizable electrolyte region with the linearized Poisson-Boltzmann implicit solvation model. The dielectric constant of water (78.4) was used. The Debye screening length was set to 3 Å, which corresponds to 1 M concentration of electrolytes evaluated by[42]

$$\lambda \approx \frac{3}{\sqrt{I}}\text{Å}$$

where *I* is the ionic strength in M. The slabs were symmetrized (inversion operation) to avoid asymmetric potential in the polarized solvation region, and the thickness of the solvent was set to 60 Å.

GCDFT and implicit solvent have been benchmarked in the literature,[43-45] which is a step ahead of the computational hydrogen electrode (CHE) model.[46] It enables the atomistic modeling of electrochemical interfaces at fixed electrode and ion potentials, incorporating experimentally controlled parameters such as chemical potentials, temperature, and solvent.[47-50] Although GCDFT suffices at this stage for our screening study, a more involved study calls for the role of explicit electrolyte and its finite-temperature dynamics to perform for a highly-performing electrode, which we currently have not yet discovered, to advance the understanding and optimization of RCC is required.

Adsorption energies calculations. The adsorption energies of the adsorbates on the metal surfaces are calculated using

$$\Delta E_{ad} = E(* ad) - E(*) - E(ad)$$

where the energy *ΔE* is from the static calculation on a single configuration using regular DFT; the symbol * denotes the metal-solvent interface, and *ad* denotes an isolated adsorbate species. Various adsorption sites and binding modes are probed to determine the most favorable binding configuration for each adsorbate. The charge of the system in electrochemical calculations was computed relative to the initial charge of the adsorbate (+1 or -1). We do not anticipate problems with open-shell systems because none of them are low-spin open-shell, i.e. they do not have multireference electronic structure character, which would be intrinsically problematic for DFT.

The static DFT energy *E* can be replaced by the GCDFT potential-dependent free energy $\Delta G(U^{SHE})$ to yield the potential-dependent free energy of adsorption:

$$\Delta G_{ad}(U^{SHE}) = \Delta G(U^{SHE}; * ad) - \Delta G(U^{SHE}; *) - E(ad)$$

We have calculated the adsorption energies for various binding modes at different sites (Figures S11-S14), identifying the most energetically favorable configurations within the range of applied potentials that are reported in Figure 3.

Catalyst preparation. In corrosion studies, Cu, Ti, Au, Ag, and Sn films were sputtered on Au coated quartz crystal. All the sputtered metal films were provided by the Oak Ridge National Laboratory to conduct experiments. The metal targets are 2-inch diameter pucks (Kurt Lesker, 99.999%). The sputtering procedure was operated at a target-to-substrate distance of 7.5 cm. The vacuum chamber was evacuated down to 5 x 10^{-7} torr for at least 3 hours before Ar gas (99.999%, AirGas) was flowed in. The pressure was set to 20 mTorr and the plasma was generated and maintained with 20W DC power supply. The thickness of all sample films was 300 nm.

In the RCE experiments, Cu and Ti cylinder electrodes were utilized. Au, Ag, and Sn catalysts were sputtered onto Ti cylinder electrodes for utilization. The Denton Vacuum Discovery 550 Sputtering system was used for the same equipped with two direct current (DC) guns and two radio frequency (RF) guns which bombard targets onto the substrates. The RF guns were used to sputter the targets on our electrodes. An initial Ar sputtering was performed to remove native oxide layers. Subsequently, a thin layer of sputtered Ti was applied onto the substrate, enhancing the adhesion of the metals to be sputtered. Following this process, catalyst metals were sputtered onto the electrodes, resulting in a thickness of 500 nm for each metal.

For electrodeposited Au cylinders, deionized water (18.2 MΩ cm) was used to prepare the electrodeposition bath with 0.01 M Chloroauric Acid ($HAuCl_4.H_2O$, 99.8%-Au, Sigma-Aldrich) and 0.5 M perchloric acid ($HClO_4$, ACS, 70%, redistilled, Alfa Aesar). The electrodeposition procedure was carried out under atmospheric conditions inside a fume hood. An Autolab PGSTAT302N potentiostat/galvanostat was used for the electrodeposition of Au in a two-electrode setup with a titanium cylinder substrate (active geometric area = 3 cm^2) as the working electrode and a graphite foil (Fischer Scientific) as the counter and reference electrode. Before the electrodeposition, the surface of the titanium cylinder substrate was polished using sandpaper (P600, 3M), rinsed thoroughly, sonicated in deionized water for 10 min, and finally dried under Ar flow. The electrodeposition of Au was carried out at a fixed current of -4 mA which was applied for 1 s for 50 cycles with a 5 s interval between each cycle, followed by a fixed current of –3 mA for 150 cycles which was applied for 1 s with a 5 s interval to deposit a compact and nanoporous Au film onto the titanium cylinder substrate.

Corrosion experiments. All electrochemical corrosion tests were carried out using fresh films sputtered on Au-coated eQCM crystals. We used a commercially available eQCM cell from Gamry with a similar setup as those reported in previous works.[51, 52] The eQCM cell shown schematically in Figure S19 allows a systematic corrosion study across different transition metal catalysts used in this work as a function of the applied potential. Corrosion rates were measured in two steps. First, a 0.099 M potassium perchlorate (Fisher Chemical, Certified ACS) and 0.001 M potassium hydroxide (Sigma Aldrich, >99.99% trace metals basis) solution was used as the stock solution. The inclusion of potassium hydroxide in this solution was deliberate and was made with the purpose of adjusting the pH to a value of 10.7. When the potential was stable after addition of the stock solution at the selected current, ammonium carbamate containing solution was introduced. The carbamate solutions of typical amines also have pH values of around 9 to 10. Corrosion rates were measured upon the addition of the ammonium carbamate (Thermo Scientific Chemicals, 98%) solution to the eQCM cell.

Electrochemical characterization. The RCC and CO_2R experiments were carried out using an RCE cell, a device previously used by our group to determine the contributions from dissolved CO_2 and CO_2-capture agent adducts for RCC on electrodeposited Ag electrodes.[7] The RCE cells allow the quantification of the partial pressure of CO_2 in the headspace of the cell during the electrochemical reduction of amine capture solutions. The RCE cell design shown in Figure S20**.** incorporates a unique configuration for precise control of mass transport within the cell. Momentum is transferred to the rotating catalyst by a follower magnet attached to the shaft of the

cylinder and situated inside the cap. This magnet tracks the motion of a driver magnet located external to the cell. This driver magnet is linked to the shaft of the MSR Rotator (Pine Research).

The cap for the working electrode part is responsible for the electrical connection and the volume of headspace is approximately 50 mL. This configuration is equipped with three threaded ports tailored to accommodate gas pipes and fittings (Swagelok) with a focus on leak prevention. Of these ports, one is dedicated to the direct injection of Ar gas into the electrolyte, while a second port functions as a conduit for gaseous products to reach an online gas chromatograph (GC, model 8610C, SRI Instruments). The last port serves the purpose of reactant introduction or extraction of liquid samples for subsequent quantitative analysis of liquid products. For consistency across all experiments, the identical flow rate of Ar gas employed in the working electrode compartment is also introduced into the counter electrode compartment. Importantly, this configuration maintains gastight integrity throughout the system.

Transport. To account for the effect of mass transport in RCC experiments, constant current experiments are carried out using an RCE cell with well-defined transport characteristics.[14] A constant current density of -12 mA cm^{-2} was applied to the five metal catalysts and the production rates for gas and liquid products were quantified at a rotation speed of 800 rpm. By maintaining the current density constant, a consistent flux of hydroxyl is generated at the cathode, resulting in a roughly constant pH environment at the electrode/electrolyte interface that simplifies the comparison of the intrinsic catalytic properties of the various metals. At 800 rpm, mass transport limitations should not be significant for the reduction of the captured CO_2 because the concentration of captured CO_2 in solution is very high (0.1M for the 0.2M ammonium carbamate electrolyte). The maximum current density that would be expected upon the reduction of the carbamate at 800 rpm would be -75.3 mA cm^{-2}. This is more than 6 times higher than the total current densities passed in these experiments. In the case that the captured CO_2 is not the source of reduction products but rather the dissolved CO_2, the expected partial current densities for the reduced products are at least 3 orders of magnitude smaller based on the partial pressures of CO_2 measured in the headspace of the cell. Nevertheless, the high surface area of the electrode (3 cm^2) and the high sensitivity of the gas chromatograph for the detection of CO_2 reduction products (sub-ppm detection and quantification for CO, CH_4, C_2H_4, and C_2H_6) enables the quantification of products even if the source of carbon is the free and dissolved CO_2 in the bulk of the electrolyte. The expectation is that if the dissolved CO_2 is the source of carbon for the reduced products, we should still observe a logarithmic increase in the partial current density of reduced products at low over potentials and eventually the reaching of a plateau in partial current at high overpotentials. Potential dependent studies were performed for Sn rotating cylinder electrodes where dissolved CO_2 is observed to be the carbon source, and where the partial current density for dissolved reduction products reaches a plateau at around a few μA cm^{-2}.

Product characterization. The GC is employed to detect and quantify gaseous products during the experiment. Injections were conducted every 20 minutes, comprising a 14-minute phase for separating products followed by a 6-minute cooling interval. Signals from the thermal conductivity detector (TCD) and flame ionization detector (FID) were gathered and compared to calibration curves. To analyze and measure liquid products, nuclear magnetic resonance spectroscopy (1D 1H NMR 500 MHz with a cryoprobe, Bruker) was utilized. A standard reference solution was

prepared, containing 52.5 mM of phenol (≥99.5%, Sigma-Aldrich) and 2.1 mM of dimethyl sulfoxide (DMSO, ≥99.9%, Sigma-Aldrich) in deuterium oxide (D_2O, 99.9%, EMD Millipore).

Acknowledgments

This material is based upon work performed by the Center for Closing the Carbon Cycle, which is supported by the U.S. Department of Energy, Office of Science, Office of Basic Energy Sciences Energy Frontier Research Centers program under Award Number DE-SC0023427.

References

1. Freyman, M.; Huang, Z.; Ravikumar, D.; Duoss, E.; Li, Y.; Baker, S.; Pang, S.; Schaidle, J., Perspective Reactive CO_2 capture: A path forward for process integration in carbon management. *Joule* **2023,** *7* (4), 631-651.
2. Siegel, R. E.; Pattanayak, S.; Berben, L. A., Reactive Capture of CO_2: Opportunities and Challenges. *ACS Catalysis* **2023,** *13* (1), 766-784.
3. Li, M.; Irtem, E.; Iglesias van Montfort, H. P.; Abdinejad, M.; Burdyny, T., Energy comparison of sequential and integrated CO_2 capture and electrochemical conversion. *Nature Communications* **2022,** *13* (1), 5398.
4. Heldebrant, D.; Kothandaraman, J.; Mac Dowell, N.; Brickett, L., Next steps for solvent-based CO_2 capture; integration of capture, conversion, and mineralisation. *Chemical Science* **2022,** *13* (22), 6445-6456.
5. Jerng, S. E.; Gallant, B. M., Electrochemical reduction of CO_2 in the captured state using aqueous or nonaqueous amines. *iScience* **2022,** *25* (7), 104558.
6. House, K.; Baclig, A.; Ranjan, M.; van Nierop, E.; Wilcox, J.; Herzog, H., Economic and energetic analysis of capturing CO_2 from ambient air. *Proceedings of the National Academy of Sciences of the United States of America* **2011,** *108* (51), 20428-20433.
7. Shen, K.; Cheng, D.; Reyes-Lopez, E.; Jang, J.; Sautet, P.; Morales-Guio, C. G., On the origin of carbon sources in the electrochemical upgrade of CO_2 from carbon capture solutions. *Joule* **2023,** *7* (6), 1260-1276.
8. Leverick, G.; Bernhardt, E. M.; Ismail, A. I.; Law, J. H.; Arifutzzaman, A.; Aroua, M. K.; Gallant, B. M., Uncovering the Active Species in Amine-Mediated CO_2 Reduction to CO on Ag. *ACS Catalysis* **2023,** *13* (18), 12322-12337.
9. Ma, H.; Ibáñez-Alé, E.; Ganganahalli, R.; Pérez-Ramírez, J.; López, N.; Yeo, B. S., Direct Electroreduction of Carbonate to Formate. *Journal of the American Chemical Society* **2023**.
10. Safipour, J.; Weber, A. Z.; Bell, A. T., Detrimental Effects of Monoethanolamine and Other Amine-Based Capture Agents on the Electrochemical Reduction of CO_2. *ACS Energy Letters* **2023**, 5012-5017.
11. Lee, G.; Li, Y.; Kim, J.; Peng, T.; Nam, D.; Rasouli, A.; Li, F.; Luo, M.; Ip, A.; Joo, Y.; Sargent, E., Electrochemical upgrade of CO_2 from amine capture solution. *Nature Energy* **2021,** *6* (1), 46-53.
12. Hori, Y.; Vayenas, C.; White, R.; GamboaAldeco, M., Electrochemical CO_2 reduction on metal electrodes. *Modern Aspects of Electrochemistry,* **2008,** (42), 89-189.
13. Bagger, A.; Ju, W.; Varela, A.; Strasser, P.; Rossmeisl, J., Electrochemical CO_2 Reduction: Classifying Cu Facets. *ACS Catalysis* **2019,** *9* (9), 7894-7899.
14. Jang, J.; Rüscher, M.; Winzely, M.; Morales-Guio, C. G., Gastight rotating cylinder electrode: Toward decoupling mass transport and intrinsic kinetics in electrocatalysis. *AIChE Journal* **2022,** *68* (5), e17605.
15. Watkins, N. B.; Schiffer, Z. J.; Lai, Y.; Musgrave, C. B., III; Atwater, H. A.; Goddard, W. A., III; Agapie, T.; Peters, J. C.; Gregoire, J. M., Hydrodynamics Change Tafel Slopes in Electrochemical CO_2 Reduction on Copper. *ACS Energy Letters* **2023**, 2185-2192.
16. Bagger, A.; Ju, W.; Varela, A.; Strasser, P.; Rossmeisl, J., Electrochemical CO_2 Reduction: A Classification Problem. *Chemphyschem* **2017,** *18* (22), 3266-3273.
17. Feaster, J.; Shi, C.; Cave, E.; Hatsukade, T.; Abram, D.; Kuhl, K.; Hahn, C.; Norskov, J.; Jaramillo, T., Understanding selectivity for the electrochemical reduction of carbon dioxide to formic acid and carbon monoxide on metal electrodes. *ACS Catalysis* **2017,** *7* (7), 4822-4827.
18. Todorova, T.; Schreiber, M.; Fontecave, M., Mechanistic understanding of CO_2 reduction reaction (CO2RR) toward multicarbon products by heterogeneous copper-based catalysts. *ACS Catalysis* **2020,** *10* (3), 1754-1768.

19. Richard, D.; Tom, M.; Jang, J.; Yun, S. G.; Christofides, P. D.; Morales-Guio, C. G., Quantifying transport and electrocatalytic reaction processes in a gastight rotating cylinder electrode reactor via integration of Computational Fluid Dynamics modeling and experiments. *Electrochimica Acta* **2023,** *440*, 141698.
20. Newman, J.; Balsara, N. P., *Electrochemical Systems.* John Wiley & Sons **2021**, 30, 11-12.
21. Kepp, K., A Quantitative Scale of Oxophilicity and Thiophilicity. *Inorganic Chemistry* **2016,** *55* (18), 9461-9470.
22. Revie, R. W., *Uhlig's corrosion handbook*. John Wiley & Sons **2011**, 51.
23. Liu J. Y.; Gong X. Q., Li R.; Shi H.; Cronin S. B.; Alexandrova A. N., (Photo)Electrocatalytic CO_2 Reduction at the Defective Anatase TiO_2 (101) Surface, *ACS Catal*ysis **2020,** 10 (7), 4048-4058.
24. Ringe, S. The importance of a charge transfer descriptor for screening potential CO_2 reduction electrocatalysts. *Nature Communications* **2023,** 14, 2598.
25. Fytianos, G.; Vevelstad, S.; Knuutila, H., Degradation and corrosion inhibitors for MEA-based CO_2 capture plants. *International Journal of Greenhouse Gas Control* **2016,** *50*, 240-247.
26. Voice, A.; Rochelle, G., Inhibitors of Monoethanolamine Oxidation in CO_2 Capture Processes. *Industrial & Engineering Chemistry Research* **2014,** *53* (42), 16222-16228.
27. Goff, G.; Rochelle, G., Oxidation inhibitors for copper and iron catalyzed degradation of monoethanolamine in CO_2 capture processes. *Industrial & Engineering Chemistry Research* **2006,** *45* (8), 2513-2521.
28. Aksu, S.; Doyle, F., Electrochemistry of copper in aqueous ethylenediamine solutions. *Journal of the Electrochemical Society* **2002,** *149* (7), B340-B347.
29. Johnson, H. E.; Leja, J., On the Potential/pH Diagrams of the Cu - NH 3 - H 2 O and Zn - NH 3 - H 2 O Systems. *Journal of The Electrochemical Society* **1965,** *112* (6), 638.
30. Strmcnik, D.; Gaberscek, M.; Pihlar, B.; Kocar, D.; Jamnik, J., Copper Dissolution in Ammonia Solutions: Identification of the Mechanism at Low Overpotentials. *Journal of the Electrochemical Society* **2009,** *156* (7), C222-C229.
31. Halpern, J., Kinetics Of The Dissolution Of Copper In Aqueous Ammonia. *Journal of the Electrochemical Society* **1953,** *100* (10), 421-428.
32. Britton, S. C.; Michael, D. G., The corrosion of tin by aqueous solutions of ammonia. *Journal of Applied Chemistry* **1955,** *5* (1), 1-9.
33. Han, K. N.; Fuerstenau, M. C., Factors influencing the rate of dissolution of gold in ammoniacal solutions. *International Journal of Mineral Processing* **2000,** *58* (1), 369-381.
34. Sluyters, J. H.; Wijnen, M. D.; van den Hul, H. J., The potential/pH diagram of silver in aqueous ammonium salt solution. *Electrochimica Acta* **1961,** *5* (1), 72-78.
35. Zhang, Z.; Kummeth, A. L.; Yang, J. Y.; Alexandrova, A. N., Inverse molecular design of alkoxides and phenoxides for aqueous direct air capture of CO_2. *Proceedings of the National Academy of Sciences* **2022**, 119 (25), e2123496119.
36. Jain, A.; Ong, S.; Hautier, G.; Chen, W.; Richards, W.; Dacek, S.; Cholia, S.; Gunter, D.; Skinner, D.; Ceder, G.; Persson, K., Commentary: The Materials Project: A materials genome approach to accelerating materials innovation. *Apl Materials* **2013,** *1* (1).
37. Hammer, B.; Hansen, L.; Norskov, J., Improved adsorption energetics within density-functional theory using revised Perdew-Burke-Ernzerhof functionals. *Physical Review B* **1999,** *59* (11), 7413-7421.
38. Grimme, S.; Antony, J.; Ehrlich, S.; Krieg, H., A consistent and accurate ab initio parametrization of density functional dispersion correction (DFT-D) for the 94 elements H-Pu. *Journal of Chemical Physics* **2010,** *132* (15).
38. Kresse, G.; Joubert, D., From ultrasoft pseudopotentials to the projector augmented-wave method. *Physical Review B* **1999,** *59* (3), 1758-1775.

40. Steinmann, S.; Michel, C.; Schwiedernoch, R.; Sautet, P., Impacts of electrode potentials and solvents on the electroreduction of CO2: a comparison of theoretical approaches. *Phys. Chem. Chem. Phys.* **2015,** *17* (21), 13949-13963.
41. Mathew, K.; Sundararaman, R.; Letchworth-Weaver, K.; Arias, T. A.; Hennig, R. G., Implicit solvation model for density-functional study of nanocrystal surfaces and reaction pathways. *Journal of Chemical Physics* **2014,** *140* (8), 084106.
42. Steinmann, S.; Sautet, P., Assessing a first-principles model of an electrochemical interface by comparison with experiment. *Journal of Physical Chemistry C* **2016,** *120* (10), 5619-5623.
43. Melander, M.M.; Kuisma, M.J.; Christensen, T.E.K.; Honkala, K., Grand-canonical approach to density functional theory of electrocatalytic systems: Thermodynamics of solid-liquid interfaces at constant ion and electrode potentials. *Journal of Chemical Physics* **2019***, 150* (4).
44. Mathew, K.; Kolluru, V.S.; Mula, S.; Steinmann, S.N.; Hennig, R.G., Implicit self-consistent electrolyte model in plane-wave density-functional theory. *Journal of Chemical Physics* **2019**, *151* (23).
45. Abidi, N.; Lim, K.R.G.; Seh, Z.W.; Steinmann, S.N., Atomistic modeling of electrocatalysis: Are we there yet?. *Wiley Interdisciplinary Reviews: Computational Molecular Science* **2021**, *11* (3), 1499.
46. Nørskov, J.K.; Rossmeisl, J.; Logadottir, A.; Lindqvist, L.R.K.J.; Kitchin, J.R.; Bligaard, T.; Jonsson, H., Origin of the overpotential for oxygen reduction at a fuel-cell cathode. *Journal of Physical Chemistry B* **2004**, *108* (46), 17886-17892.
47. Weitzner, S.E.; Akhade, S.A.; Varley, J.B.; Wood, B.C.; Otani, M., Baker, S.E.; Duoss, E.B., Toward engineering of solution microenvironments for the CO2 reduction reaction: unraveling pH and voltage effects from a combined density-functional–continuum theory. *Journal of Physical Chemistry Letters* **2020**, *11* (10), 4113-4118.
48. Wu, T.; Melander, M.M.; Honkala, K., Coadsorption of NRR and HER intermediates determines the performance of Ru-N4 toward electrocatalytic N2 reduction. *ACS Catalysis* **2022**, *12* (4), 2505-2512.
49. Zhang, Z.; Li, J.; Wang, Y.G., Modeling Interfacial Dynamics on Single Atom Electrocatalysts: Explicit Solvation and Potential Dependence. *Accounts of Chemical Research* 2024, *57* (2), 198-207.
50. Cheng, D.; Alexandrova, A.N.; Sautet, P., H-Induced Restructuring on Cu (111) Triggers CO Electroreduction in an Acidic Electrolyte. *Journal of Physical Chemistry Letters* **2024**, *15*, 1056-1061.
51. Scivetti, I.; Teobaldi, G., ALC_EQCM: Automated stoichiometric resolution in electrochemistry through Density Functional Theory aided, Electrochemical Quartz Crystal Microbalance. *Computational Materials Science* **2023,** *218*.
52. Rahmouni, K.; Keddam, M.; Srhiri, A.; Takenouti, H., Corrosion of copper in 3% NaCl solution polluted by sulphide ions. *Corrosion Science* **2005,** *47* (12), 3249-3266.